

Article

Constant Wear Criterion for Optimization of the Crushing Chamber of Cone Crushers

Zilong Zhang ^{*}, Tingzhi Ren and Jiayuan Cheng

National Engineering Research Center for Equipment and Technology of Cold Rolled Strip, Yanshan University, Qinhuangdao 066004, China; tingzhirenwork@gmail.com (T.R.); jiayuanchengwork@gmail.com (J.C.)

* Correspondence: zhangzilong0630@163.com

Abstract: The crushing chamber is the core component of a cone crusher, consisting of mantle and concave parts. Reducing the impact of crushing chamber wear on the performance of cone crushers and the quality of crushed products while extending the service life of the mantle and concave has become a significant research challenge. The impact of the compression ratio and particle size distribution coefficient on the particle crushing pressure is investigated here in order to establish the particle pressure model. The effect of the normal and tangential components of particle crushing pressure on the wear of the mantle and concave is discussed, and the wear with the increase in crushed products and accumulation of operating time is explored in order to develop a wear model of the crushing chamber. By evaluating the compensation of the worn crushing chamber according to the adjustment mechanism of the mantle, a constant wear criterion for the crushing chamber of the cone crusher is proposed. Through analysis of industrial experimental data on an experimental prototype of a ZS200MF cone crusher with an optimized mantle and concave, the capacity was found to fluctuate at 83.45 t/h with no apparent downward trend, the calibration size production was reduced by 6.2%, and the wear similarity coefficient was 8.82%. This indicates that replacing the optimized mantle and concave based on the constant wear criterion maintains the performance of the cone crusher, delays the decline in the quality of the crushed products, and ensures similarity between the adjusted worn crushing chamber and the initial crushing chamber, which verifies the feasibility and effectiveness of the constant wear criterion for the optimization of crushing chamber. Based on the constant wear criterion, cone crushers can be optimized to obtain a crushing chamber with constant wear characteristics, which provides theoretical support for the development of new high-efficiency cone crushers as well as the optimization of existing equipment.



Citation: Zhang, Z.; Ren, T.; Cheng, J. Constant Wear Criterion for Optimization of the Crushing Chamber of Cone Crushers. *Minerals* **2022**, *12*, 807. <https://doi.org/10.3390/min12070807>

Academic Editor: Luís Marcelo Tavares

Received: 20 May 2022

Accepted: 23 June 2022

Published: 24 June 2022

Publisher's Note: MDPI stays neutral with regard to jurisdictional claims in published maps and institutional affiliations.



Copyright: © 2022 by the authors. Licensee MDPI, Basel, Switzerland. This article is an open access article distributed under the terms and conditions of the Creative Commons Attribution (CC BY) license (<https://creativecommons.org/licenses/by/4.0/>).

1. Introduction

Cone crushers are high-efficiency particle crushing instruments utilized in a variety of industries [1]. The crushing chamber is one of the core components of a cone crusher [2], and is directly related to the performance of the cone crusher and the quality of the crushed products. Meanwhile, changes in the crushing chamber caused by wear can significantly impact the economic efficiency of crushing equipment. An effective criterion for optimizing the crushing chamber that reduces the impact of wear on the performance of cone crushers and the quality of crushed products while extending the service life of the crushing chamber is required, and can provide theoretical guidance for the development of long service life crushing chambers and a resulting reduction in operating costs. As a result, this work has significant theoretical value and practical significance.

The particle crushing pressure and the wear mechanism of crushing chambers have been extensively investigated by many scholars. Archard [3] proposed a model for estimating surface wear in which the wear is assumed to be proportional to the pressure on the surface and the relative sliding distance. Page et al. [4] and Yao et al. [5] investigated

the wear of silica sand on metal surfaces using an experimental method and refined the method of obtaining the required wear coefficient in the Archard model [3]. Yang et al. [6] developed a calculation method based on hertz contact theory and the Archard wear model for the wear of the split cone of a vertical shaft impact crusher. Lindqvist et al. [7] developed a quantitative model of the particle crushing pressure for the wear in jaw crushers, concluding that the wear on the crushing chamber is proportional to the maximum crushing pressure, and analyzed the wear characteristics of cone crushers based on this model [8]. Lindqvist et al. [9,10] investigated the effect of the particle size of the crushed particles on the wear by examining experiments in which two counter-rolled steel wheels squeezed silica sand with different sizes. Based on Lindqvist's research foundation and through the study of particle crushing pressure models, Dong et al. [11,12] developed a cone crusher wear model able to predict the wear trend of the crushing chamber. Repone et al. [13] conducted an experiment on the wear characteristics of a crushing chamber made of different materials during the operation of cone crushers, which was carried out using Metso mining machinery. Xu et al. [14] proposed a model to predict lining wear based on a shear impact energy model. Juuso et al. [15] investigated the relationship between the wear on the crushing chamber and the capacity of the cone crusher using a modified Archard wear equation. Liu et al. [16] proposed a general model to explore the relationship between cone crusher parameters and liner wear by considering the relative sliding and pressure between particles and the liner. Based on the discrete element method, Cleary et al. [17,18] and Sinnott et al. [19] investigated the relationship between the particle crushing pressure distribution and the amount of wear in the crushing chamber by analyzing the particle crushing pressure with different physical parameters. Bengtsson et al. [20] and Hulthén et al. [21,22] created a wear model of a cone crusher and simulated the wear deformation of the crushing chamber. Li et al. [23] examined the functional relationship between liner wear and cone crusher structure parameters by simulating the crushing process of different-shaped particles. Duan et al. [24] simulated the crushing process of a single particle in a cone crusher, calculated the wear amount on the liner at each stage of the life cycle, and compared the results with the experimental data of the Ansteel Group. Although existing models have allowed for extensive research to be conducted on the wear mechanism of metal planes and the performance of certain analyses on the wear law of the crushing chamber, there have been no investigations into adjustments to worn crushing chambers based on the particular structure of the cone crusher. Thus, an effective criterion for extending the service life of the crushing chamber based on reducing the effect of wear on the performance of cone crushers and the quality of crushed products has not yet been proposed. As a result, it is necessary to establish a criterion for extending the service life of crushing chambers based on analysis of the wear process in the cone crusher crushing chamber.

Here, the particle crushing process in the crushing chamber was simulated via the secondary crushing of particles with different compression ratios. The influence of the compression ratio and particle size distribution coefficient on the particle crushing pressure was investigated, and a particle crushing pressure model was established. The effect of the normal and tangential components of the particle crushing pressure on the wear of mantle and concave was explored. The wear with an increasing volume crushed particles and accumulation of operating time was considered, and a wear model of the crushing chamber was developed. Based on this wear model, the similarity between the adjusted worn crushing chamber and the crushing chamber without wear is discussed. A constant wear criterion with the wear similarity coefficient as the optimization objective function was proposed. The proposed constant wear criterion was adopted in order to optimize the crushing chamber, which extended the service-life of the crushing chamber while reducing the impact on both the performance of the cone crusher and the quality of the crushed product. This provides a theoretical foundation for the development of wear-resistant crushing chambers for high-efficiency cone crushers.

2. Particle Crushing Pressure Model of the Crushing Chamber

The crushing chamber of a cone crusher is composed of the mantle and concave. The particles in the crushing chamber are crushed by the squeezing of the mantle and concave. In this process, the mantle and concave directly contact the particles, and are gradually worn down due to the enormous crushing pressure and intense impact. As a result, in order to evaluate the wear on the mantle and concave in detail, it is necessary to analyze the particle crushing pressure in the crushing chamber.

2.1. Particle Crushing Pressure Experiment

According to the particle crushing experiment conducted by Lindqvist [7], the particle crushing pressure increases with the increasing compression degree of the particles. In the particle crushing process, because the particles in the crushing chamber are a mixture of various sizes, the bulk properties of particles inevitably affect the particle crushing pressure. As a result, the particle crushing pressure is related to the compression degree and bulk properties of particles. Here, the particle size distribution coefficient σ and the compression ratio ε were selected as the research objects of the particle crushing pressure experiment. The particle size distribution coefficient σ characterizes the uniformity of the particle size distribution [25], and the compression ratio ε represents the proportional relationship between the compression volume and the initial volume:

$$\sigma = \frac{\sqrt{\sum_{i=1}^k p_i (\bar{d}_i - \bar{d})^2}}{\bar{d}} \quad (1)$$

$$\bar{d} = \sum_{i=1}^k p_i \bar{d}_i \quad (2)$$

$$\varepsilon = \frac{s}{b} \quad (3)$$

where p_i is the mass percentage of particles in the i -th particle size, \bar{d}_i is the average particle size in the i -th particle size, \bar{d} is the average particle size considering the mass percentage, s is the compression volume, and b is the initial volume.

Particles with a certain size were loaded into an experimental cylinder and crushed with a predetermined compression ratio. The crushed particles were sieved and weighed, then reloaded into the experimental cylinder for a second crushing with the same compression ratio. Thus, the crushing process of particles with different sizes in the crushing chamber subjected to squeezing with different compression degrees was simulated. The particle size distribution coefficient σ and compression ratio ε were selected as the experimental parameters, and the experimental values of the parameters were determined within a reasonable range according to the performance of the cone crusher and the geometry of the crushing chamber. The particles were loaded into the experimental cylinder and placed on the working platform of the hydraulic press. The particles in the experimental cylinder were crushed by the hydraulic press. The crushed particles were sieved using a standard stone sieve. The masses of crushed particles with different sizes were weighed, and the particle size distribution coefficient σ of the crushed particles was obtained. The crushed particles were remixed and reloaded into the experimental cylinder, and a second crushing was carried out with the same compression ratio ε as the first crushing. Then, a series of experimental data on the particle crushing pressure were obtained. The experimental process is shown in Figure 1. The experimental equipment and results are shown in Figure 2. The physical parameters of the experiment particles are shown in Table 1. The detailed steps of the particle crushing pressure experiment are described below.

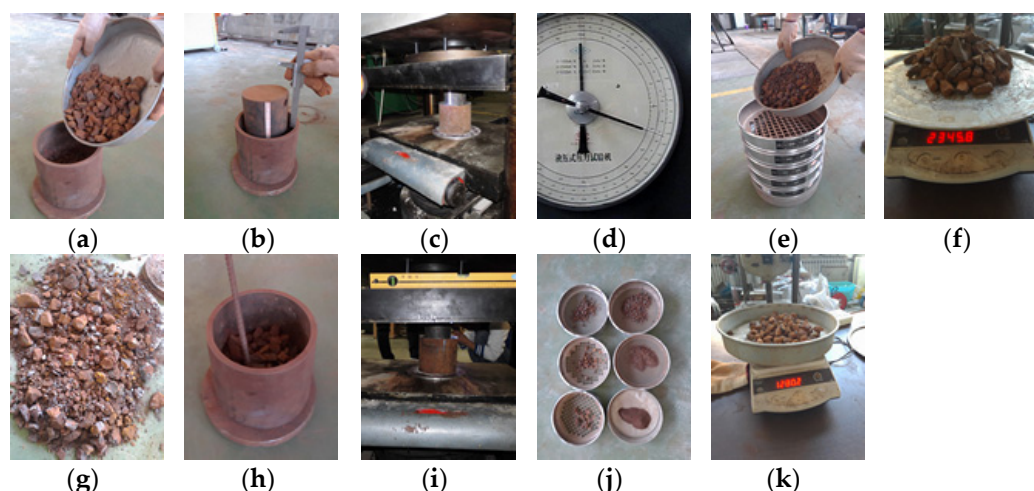


Figure 1. The steps of the particle crushing pressure experiment: (a) the particles are loaded into the experimental cylinder; (b) the indenter is arranged; (c) the particles are crushed by the hydraulic press; (d) the particle crushing pressure is achieved; (e) the crushed particles are screened using standard stone sieves; (f) the masses of crushed particles in each size are weighed by an electronic scale; (g) the crushed particles with different sizes are mixed; (h) the mixed particles are reloaded into the experimental cylinder; (i) the mixed particles are crushed again; (j) the crushed particles are screened again; (k) the masses of crushed particles in each size are weighed.

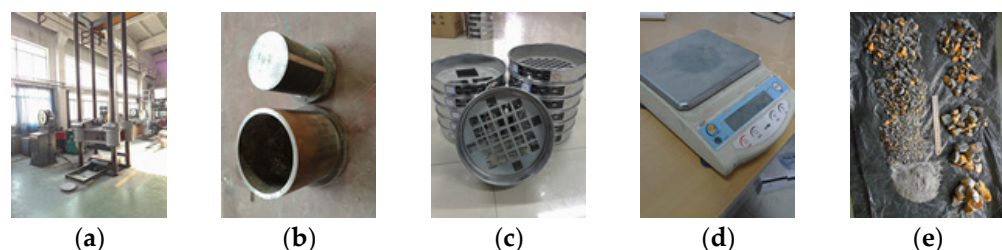


Figure 2. The experimental equipment and result: (a) hydraulic press; (b) indenter and experimental cylinder; (c) standard stone sieves; (d) electronic scale; (e) crushed particles with different sizes.

Table 1. The physical parameters of the experimental particles.

Parameter	Unit	Value
Material		Magnetite
Composition		Fe_3O_4
Mohs hardness (HM)		5.9
Compressive strength (σ)	Mpa	137
Tap density (ρ_T)	t/m ³	4.9
Pack density (ρ_P)	t/m ³	2.8
Moisture content (w)	%	3.6

Step 1. Particles with a size of 25–31.5 mm were selected as experimental material using the standard stone sieve. After loading into the experimental cylinder, the particles were leveled to allow the horizontal error of the particle surface to be controlled to 1 mm. The loading height b of the particles in the experimental cylinder was determined using a vernier caliper.

Step 2. The indenter was arranged on the experimental cylinder. The experimental cylinder was placed on the bottom working platform of the hydraulic press. The compression length was calculated according to the loading height b of the particles in the experimental cylinder and the preset compression ratio ($\varepsilon = 0.5$).

Step 3. Through the control system of the hydraulic press and the scale on the indenter, the particles in the experimental cylinder were crushed steadily by the indenter at a constant speed.

Step 4. As the indenter reached the preset compression length, the particle crushing pressure in the experimental cylinder was read using the scale plate of the hydraulic press.

Step 5. The upper working platform of the hydraulic press was raised. The indenter in the experimental cylinder was removed. The height of particles in the experimental cylinder was measured using a vernier caliper. The crushed particles were screened using standard stone sieves, and the masses of crushed particles with different sizes were weighed using an electronic scale. The particle size distribution coefficient σ of the crushed particles was obtained.

Step 6. The crushed particles with different sizes were mixed evenly and reloaded into the experimental cylinder. The mixed crushed particles were crushed again with the same compression ratio. The particle crushing pressure was determined according to the scale plate of the hydraulic press. The crushed particles were sieved and weighed to obtain the particle size distribution coefficient σ of the crushed particles.

Step 7. The compression ratio ϵ was changed to 0.1, 0.15, 0.2, 0.25, 0.3, and 0.35, and Steps 1–6 were repeated. The experimental data on the particle crushing pressure were obtained and recorded in Table 2, then the particle crushing pressure experiment finished.

Table 2. The experimental data of the particle crushing pressure.

Parameter	Size	Height	Stoke	Compression Ratio	Size Distribution Coefficient	Particle Crushing Pressure
	<i>d</i>	<i>b</i>	<i>s</i>	ϵ	σ	<i>p</i>
Unit	mm	mm	mm	-	-	Mpa
1	26.5–31.5	82.3	8.2	0.099	0.021	3.276
2	From Unit 1	77.2	7.9	0.102	0.165	3.813
3	26.5–31.5	80.4	9.1	0.113	0.019	3.652
4	From Unit 3	73.5	7.5	0.102	0.182	3.871
5	26.5–31.5	76.2	12.3	0.161	0.012	5.296
6	From Unit 5	65	9.4	0.144	0.235	5.649
7	26.5–31.5	84.6	12.1	0.143	0.03	4.67
8	From Unit 7	75.2	11.5	0.152	0.241	6.048
9	26.5–31.5	75.9	14.5	0.191	0.015	6.726
10	From Unit 9	62.9	13	0.206	0.272	9.512
11	26.5–31.5	80.3	16	0.199	0.009	7.125
12	From Unit 11	66.2	13.1	0.197	0.286	8.972
13	26.5–31.5	78.5	18.9	0.24	0.015	9.893
14	From Unit 13	61.8	15.6	0.252	0.332	14.414
15	26.5–31.5	76.8	18.8	0.244	0.019	10.246
16	From Unit 15	60	15.6	0.26	0.361	15.752
17	26.5–31.5	83.2	25.4	0.305	0.01	16.433
18	From Unit 17	60.9	18.9	0.31	0.369	23.52
19	26.5–31.5	79.5	24.9	0.313	0.005	17.424
20	From Unit 19	56	17.1	0.305	0.388	22.997
21	26.5–31.5	75.6	26.1	0.345	0.015	22.618
22	From Unit 21	51.2	17.4	0.339	0.412	30.706
23	26.5–31.5	79.8	27	0.338	0.022	21.538
24	From Unit 23	53.5	19.2	0.358	0.402	35.347

Our analysis of the particle crushing pressure experimental data found that the particle crushing pressure p is proportional to the particle size distribution coefficient σ . Meanwhile, when the compression ratio ϵ increases, the particle crushing pressure p grows rapidly, with an exponential changing trend. As a result, the particle crushing pressure model can be

established by non-linear fitting of the particle crushing pressure experimental data, as expressed by Equation (4):

$$p = (a_1\sigma + a_2)\exp(a_3\varepsilon + a_4) \quad (4)$$

$$a_1 = 0.912 \quad a_2 = -0.074 \quad a_3 = 1.451 \quad a_4 = 4.268$$

where a_1 , a_2 , a_3 , and a_4 are the fitting coefficient of the particle crushing pressure model.

According to the particle crushing pressure model expressed in Equation (4), the simulation of the particle crushing pressure model is shown in Figure 3.

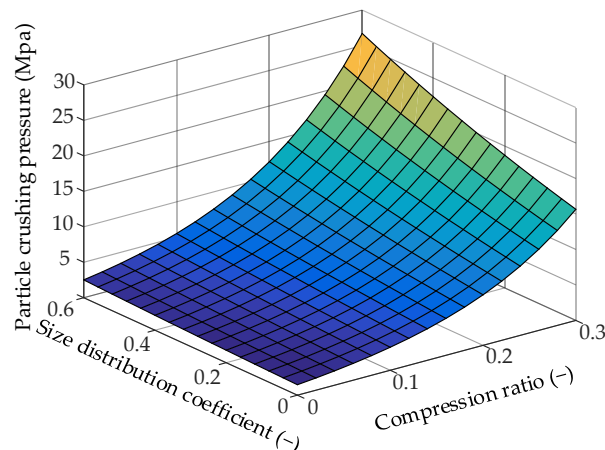


Figure 3. The simulation of the particle crushing pressure model.

As shown in Figure 3, the particle crushing pressure is proportional to the compression ratio. As the compression ratio increases, the particle crushing pressure increases exponentially. As the particles are filled with voids at the initial stage of crushing, the particle crushing pressure gradually increases as the compression ratio increases. With the further crushing of the particles, the particles are gradually deformed and crushed. The particle crushing pressure increases sharply with the increase in the compression ratio. The particle crushing pressure increases with the increase in the particle size distribution coefficient. The main reason for this is that those particles with a larger size distribution coefficient have a more uneven distribution. Certain particles have a larger size, while others have a relatively small size. The voids between particles with a larger size become filled by particles with a small size, and the “dense effect” is more obvious in the process of particle crushing, which leads to an increase in the particle crushing pressure.

2.2. Particle Crushing Pressure Distribution in the Crushing Chamber

Based on the particle crushing pressure model, the particle crushing pressure distribution in the crushing chamber can be simulated. During operation of a cone crusher, the particles are fed into the crushing chamber from the feeding port. After several crushings, the particles are discharged from the crushing chamber. According to the structural and operating parameters of the cone crusher, the motion characteristics of particles in the crushing chamber can be determined such that the path of the particles in the crushing chamber can be obtained [26]. Then, the crushing chamber can be divided into several crushing zones, as shown in Figure 4.

The mantle rotates eccentrically around the central axis of the cone crusher. As the mantle moves from the concave to the limit position, the surface OSS (Open Side Setting) of the mantle is formed. As the mantle moves towards the concave to the limit position, the surface CSS (Closed Side Setting) of the mantle is formed. When the particles pass through any of the crushing zones they are crushed by a single squeeze of the mantle and concave, which leads to the direct effect of the particle crushing pressure on the mantle and concave of the current crushing zone. Based on the particle crushing pressure model, the

particle crushing pressure in any crushing zone is determined by the compression ratio of the crushing zone and the size distribution coefficient of the crushed particles. The compression ratio is determined by the structural and operating parameters of the cone crushers. The size distribution coefficient is determined by the feed bulk properties of the cone crusher. As a result, the particle crushing pressure distribution of the crushing chamber is related to the structural and operating parameters and feed bulk properties of the cone crusher.

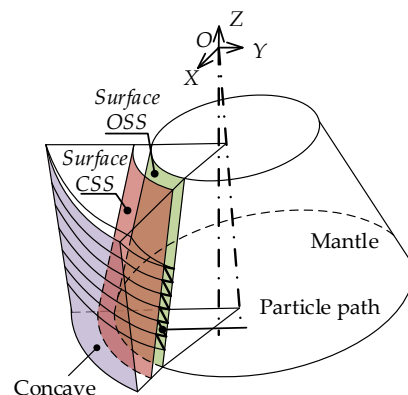


Figure 4. The division of the crushing chamber according to the path of particles.

As shown in Figure 5, in the i -th crushing zone of the crushing chamber the particles dynamically fill the whole crushing zone. When the mantle rotates the central axis of the cone crusher for a week, the particles in the i -th crushing zone are crushed once. According to the definition of the compression ratio, the volume of particles before compression is V_{int} . After crushing, the volume of the particles is V_{end} . The volume of particles in the i -th crushing zone decreases V_{com} during this crushing, and the compression ratio in the i -th crushing zone can be expressed as

$$\varepsilon_i = \frac{s}{b} = \frac{V_{com}}{V_{int}} = \frac{V_{int} - V_{end}}{V_{int}} \quad (5)$$

where ε_i is the compression ratio in the i -th crushing zone.

Based on the improved model of inter-particle breakage considering the transformation of the particle shape for the cone crusher [27–29], the crushing process of particles in the crushing chamber was simulated by measuring the feed bulk properties of the cone crusher and calculating the compression ratio of each crushing zone in the crushing chamber. Based on the particle crushing pressure model, the particle crushing pressure distribution of the mantle and concave can be obtained according to the compression ratio and particle size distribution coefficient of each crushing zone in the crushing chamber, as shown in Figure 6.

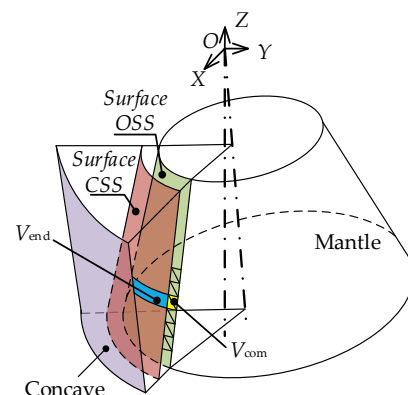


Figure 5. The volume change of the crushing zone.

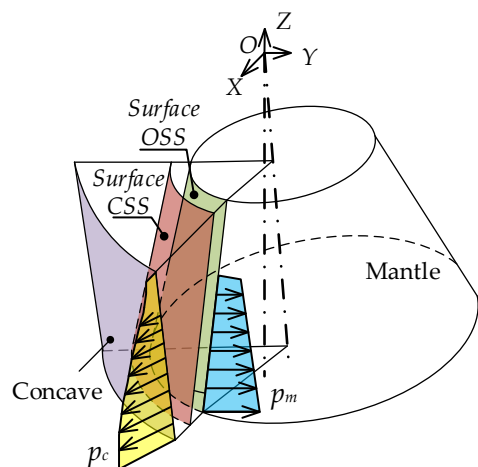


Figure 6. The particle crushing pressure distribution in crushing chamber.

As shown in Figure 6, the particle crushing pressure on the mantle and concave gradually increase with the decrease in height, which is determined by the geometry of the crushing chamber and the bulk properties of the crushed particles. The compression ratio in the crushing chamber increases as the height of the crushing chamber decreases due to the eccentric rotation motion of the mantle and the geometry of the crushing chamber, which is “large on top and small on bottom.” As the particles are crushed several times in the crushing chamber, the particle size distribution becomes more uniform. The particle size distribution coefficient of the crushing zone decreases with the reduction in the height. According to Equation (4), the compression ratio has a more substantial influence on the particle crushing pressure than the particle size distribution coefficient, resulting in the particle crushing pressure increasing as the height of the crushing chamber decreases.

3. Wear Model of the Crushing Chamber

The mantle and concave are directly involved in the crushing process of particles, which are affected by the particle crushing pressure and the impact of crushed particles with different sizes. Therefore, with increasing crushed particles and accumulated operating time, the mantle and concave are worn down. This wear is mainly related to the material of the crushing chamber, the physical parameters of the crushed particles, the distribution of the particle crushing pressure, etc. The wear on the crushing chamber along the height direction is directly related to the particle crushing pressure distribution.

The decomposition of the particle crushing pressure can be analyzed according to the particular geometry of the crushing chamber, as shown in Figure 7.

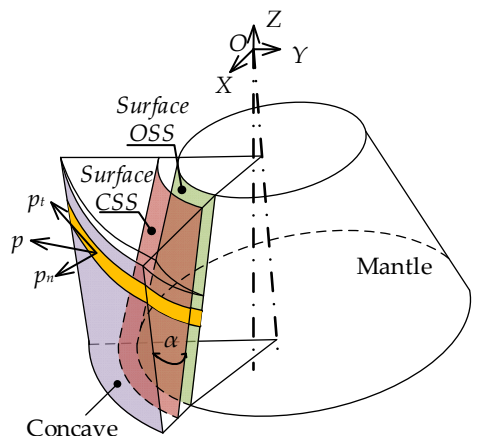


Figure 7. The decomposition of the particle crushing pressure.

As shown in Figure 7, when the particles are crushed by the mantle and concave in the crushing chamber, the particle crushing pressure p can be divided into a normal component p_n perpendicular to the mantle and concave and a tangential component p_τ along the tangential plane of the mantle and concave, as shown in Equations (6) and (7):

$$p_n = \frac{p}{\sqrt{1 + (\tan \frac{\alpha}{2})^2}} \quad (6)$$

$$p_\tau = \frac{p \tan \frac{\alpha}{2}}{\sqrt{1 + (\tan \frac{\alpha}{2})^2}} \quad (7)$$

where α is the pressure angle of the crushing chamber.

According to the motion characteristics of the particles and the mantle, the crushing zones in the crushing chamber are perpendicular to the surface CSS. In the i -th crushing zone of the crushing chamber, the normal and tangential components of the particle crushing pressure on the mantle can be expressed as

$$p_{n,i}^m = p_i \quad (8)$$

$$p_{\tau,i}^m = 0 \quad (9)$$

where $p_{n,i}^m$ is the normal component of the particle crushing pressure on the mantle in the i -th crushing zone, $p_{\tau,i}^m$ is the tangential component of the particle crushing pressure on the mantle in the i -th crushing zone, and p_i is the particle crushing pressure in the i -th crushing zone.

Similarly, the normal and tangential components of the particle crushing pressure on the concave in the i -th crushing zone of the crushing chamber can be expressed as

$$P_{n,i}^c = \frac{P_i}{\sqrt{1 + (\tan \frac{\alpha_i}{2})^2}} \quad (10)$$

$$P_{\tau,i}^c = \frac{P_i \tan \frac{\alpha_i}{2}}{\sqrt{1 + (\tan \frac{\alpha_i}{2})^2}} \quad (11)$$

where $P_{n,i}^c$ is the normal component of the particle crushing pressure on the concave in the i -th crushing zone, $P_{\tau,i}^c$ is the tangential component of the particle crushing pressure on the concave in the i -th crushing zone, and α_i is the pressure angle in the i -th crushing zone of the crushing chamber.

During the crushing process, the mantle and concave are worn down with the increase in crushing particle and the accumulation of operating time [30]. The wear in the perpendicular direction of the mantle and concave can be expressed as

$$\Delta w_i^m = \frac{p_{n,i}^m + K p_{\tau,i}^m}{W} \mu \int_0^t m(t) dt \quad (12)$$

$$\Delta w_i^c = \frac{p_{n,i}^c + K p_{\tau,i}^c}{W} \mu \int_0^t m(t) dt \quad (13)$$

where Δw_i^m is the wear of the mantle in the i -th crushing zone, Δw_i^c is the wear of the concave in the i -th crushing zone, K is the tangential correction coefficient, W is the wear resistance coefficient of the crushing chamber, μ is the wear coefficient, and $m(t)$ is the mass of the crushed particles, which varies with the operating time of the cone crusher.

4. Constant Wear Criterion for the Crushing Chamber of the Cone Crusher

As huge amounts of particles are crushed in the crushing chamber, the service conditions of the mantle and concave involved in the crushing process become abominable. The

mantle and concave are worn down to different degrees. With the increasing wear of the mantle and concave, the geometry of the crushing chamber changes, which has a substantial impact on the performance of the cone crusher and the quality of the crushed products. As a result, a thorough examination of the wear characteristics and the adjustment law of the crushing chamber is required, as is the establishment of a crushing chamber criterion.

As shown in Figure 8, a hydraulic cone crusher with a single hydraulic cylinder at the bottom is taken as an example. The concave is fixed on the shell. The mantle is installed on the main shaft, where the upper end is fixed by a spherical plain bearing and the lower end is supported by the hydraulic cylinder. As the crushing chamber is worn down, the geometry of the crushing chamber changes, reducing the performance of the cone crusher and the quality of the crushed products. Therefore, the worn crushing chamber must be adjusted. Hydraulic oil is injected into the bottom hydraulic cylinder, causing the main shaft which is in contact with the bottom hydraulic cylinder to travel upwards under the constraint of the spherical plain bearing. The increase in the height of the mantle compensates for the wear of the crushing chamber caused by particle crushing. Thus, the CSS size of the discharge port is adjusted and the length of the parallel zone is extended.

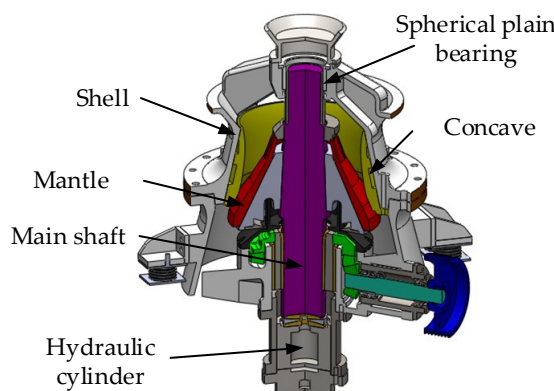


Figure 8. The structure of a hydraulic cone crusher with a single hydraulic cylinder at the bottom.

As shown in Figure 9, the crushing chamber of the cone crusher is divided into several crushing zones according to the motion characteristics of the particles. The control points on the mantle and concave that are utilized to divide each crushing zone are as follows: $P_1^c, P_2^m \dots P_i^m, P_{i+1}^m \dots P_{k+1}^m, P_1^c, P_2^c \dots P_i^c, P_{i+1}^c \dots P_{k+1}^c$. The i -th crushing zone of the crushing chamber is composed of the mantle control points P_i^m, P_{i+1}^m and the concave control points P_i^c, P_{i+1}^c . As huge amounts of particles are crushed in the crushing chamber, the mantle and concave both become worn down.

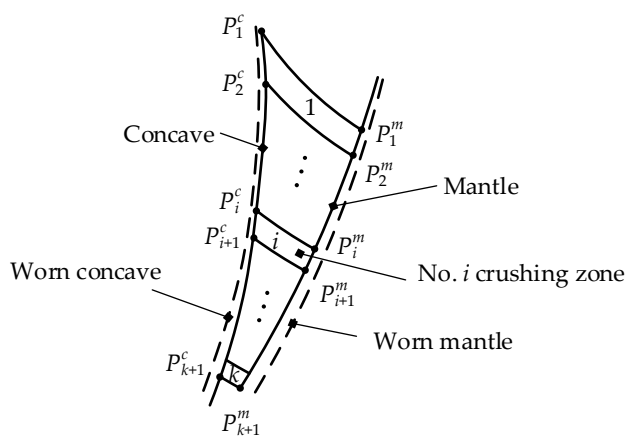


Figure 9. The wear of the mantle and concave in the crushing chamber.

The i -th crushing zone in the crushing chamber was selected as the research object. Based on the wear model of the crushing chamber, the worn mantle and concave in the i -th crushing zone are shown in Figure 10 when the mass of particles m is crushed by the mantle and concave at time t .

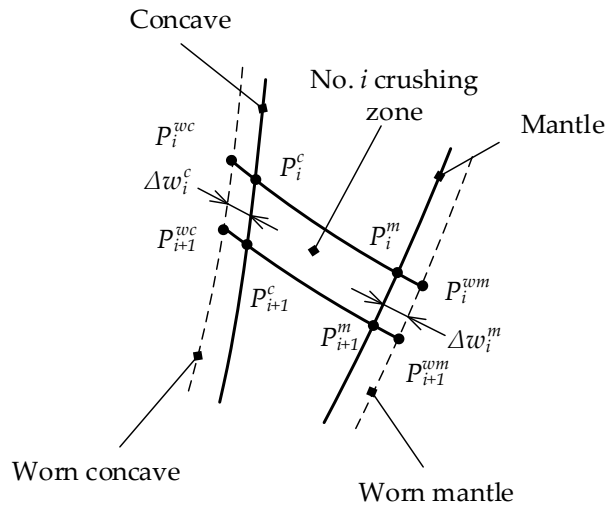


Figure 10. The wear of the mantle and concave in the i -th crushing zone.

In any crushing zone, the worn mantle and concave are parallel to the mantle and concave without wear. When the i -th crushing zone is worn down, the control points P_i^m and P_{i+1}^m , which make up the mantle, are worn down to control points P_i^{wm} and P_{i+1}^{wm} with the amount of wear Δw_i^m . Meanwhile, the control points P_i^c and P_{i+1}^c , which make up the concave, are worn down to the control points P_i^{wc} and P_{i+1}^{wc} with the wear amount Δw_i^c . According to the control point coordinates of the mantle and concave in the i -th crushing zone without wear, the control point coordinates of the worn mantle and concave can be calculated, and are expressed as

$$P_{i,x}^{ww} = \frac{\left(P_{i,y}^m - P_{(i+1),y}^m \right) \Delta w_i^m}{\sqrt{\left(P_{i,x}^m - P_{(i+1),x}^m \right)^2 + \left(P_{i,y}^m - P_{(i+1),y}^m \right)^2}} + P_{i,x}^m \quad (14)$$

$$P_{i,y}^{wm} = -\frac{\left(P_{i,x}^m - P_{(i+1),x}^m \right) \Delta w_i^m}{\sqrt{\left(P_{i,x}^m - P_{(i+1),x}^m \right)^2 + \left(P_{i,y}^m - P_{(i+1),y}^m \right)^2}} + P_{i,y}^m \quad (15)$$

$$P_{(i+1),x}^{wm} = \frac{\left(P_{i,y}^m - P_{(i+1),y}^m \right) \Delta w_i^m}{\sqrt{\left(P_{i,x}^m - P_{(i+1),x}^m \right)^2 + \left(P_{i,y}^m - P_{(i+1),y}^m \right)^2}} + P_{(i+1),x}^m \quad (16)$$

$$P_{(i+1),y}^{wm} = -\frac{\left(P_{i,x}^m - P_{(i+1),x}^m \right) \Delta w_i^m}{\sqrt{\left(P_{i,x}^m - P_{(i+1),x}^m \right)^2 + \left(P_{i,y}^m - P_{(i+1),y}^m \right)^2}} + P_{(i+1),y}^m \quad (17)$$

$$P_{i,x}^{wc} = -\frac{\left(P_{i,y}^c - P_{(i+1),y}^c \right) \Delta w_i^c}{\sqrt{\left(P_{i,x}^c - P_{(i+1),x}^c \right)^2 + \left(P_{i,y}^c - P_{(i+1),y}^c \right)^2}} + P_{i,x}^c \quad (18)$$

$$P_{i,y}^{wc} = \frac{\left(P_{i,x}^c - P_{(i+1),x}^c\right)\Delta w_i^c}{\sqrt{\left(P_{i,x}^c - P_{(i+1),x}^c\right)^2 + \left(P_{i,y}^c - P_{(i+1),y}^c\right)^2}} + P_{i,y}^c \quad (19)$$

$$P_{(i+1),x}^{wc} = -\frac{\left(P_{i,y}^c - P_{(i+1),y}^c\right)\Delta w_i^c}{\sqrt{\left(P_{i,x}^c - P_{(i+1),x}^c\right)^2 + \left(P_{i,y}^c - P_{(i+1),y}^c\right)^2}} + P_{(i+1),x}^c \quad (20)$$

$$P_{(i+1),y}^{wc} = \frac{\left(P_{i,x}^c - P_{(i+1),x}^c\right)\Delta w_i^c}{\sqrt{\left(P_{i,x}^c - P_{(i+1),x}^c\right)^2 + \left(P_{i,y}^c - P_{(i+1),y}^c\right)^2}} + P_{(i+1),y}^c \quad (21)$$

where $P_{i,x}^{wm}$, $P_{i,y}^{wm}$, $P_{(i+1),x}^{wm}$, and $P_{(i+1),y}^{wm}$ are the x and y coordinates of the control point of the worn mantle in the i -th crushing zone, $P_{i,x}^{wc}$, $P_{i,y}^{wc}$, $P_{(i+1),x}^{wc}$, and $P_{(i+1),y}^{wc}$ are the x and y coordinates of the control point of the worn concave in the i -th crushing zone, $P_{i,x}^m$, $P_{i,y}^m$, $P_{(i+1),x}^m$, and $P_{(i+1),y}^m$ are the x and y coordinates of the control point of the mantle without wear in the i -th crushing zone, and $P_{i,x}^c$, $P_{i,y}^c$, $P_{(i+1),x}^c$, and $P_{(i+1),y}^c$ are the x and y coordinates of the control point of the concave without wear in the i -th crushing zone.

Hydraulic oil is injected into the hydraulic cylinder at the bottom of the cone crusher, causing the mantle installed on the main shaft to lift. Thus, the wear on the crushing chamber is compensated for by adjusting the mantle, as shown in Figure 11. By adjusting the height of the mantle, the control points of the mantle in the i -th crushing zone are adjusted to P_i^{am} and P_{i+1}^{am} . The adjusted control point coordinates are shown in Equations (22)–(25).

$$P_{i,x}^{am} = P_{i,x}^{wm} + h \tan(\theta) \quad (22)$$

$$P_{i,y}^{am} = P_{i,y}^{wm} + h \quad (23)$$

$$P_{(i+1),x}^{am} = P_{(i+1),x}^{wm} + h \tan(\theta) \quad (24)$$

$$P_{(i+1),y}^{am} = P_{(i+1),y}^{wm} + h \quad (25)$$

where $P_{i,x}^{am}$, $P_{i,y}^{am}$, $P_{(i+1),x}^{am}$, and $P_{(i+1),y}^{am}$ are the x and y coordinates of the central point of the adjusted worn mantle in the i -th crushing zone.

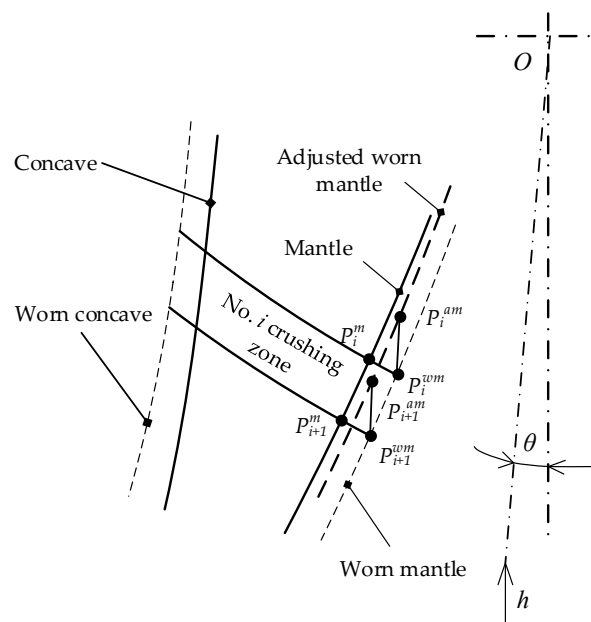


Figure 11. The adjustment of the worn mantle in the i -th crushing zone.

The performance of the cone crusher and the quality of the crushed products are related to the operating parameters of the cone crusher, the geometry of the crushing chamber, and the bulk properties of the feed. Because the cone crusher operates continuously, the operating parameters and the bulk properties of the feed do not change. During continuous operation of the cone crusher, huge amounts of particles are crushed in the crushing chamber. The mantle and concave of the crushing chamber are continuously worn down, resulting in a change in the geometry of the crushing chamber. This change in the geometry of the crushing chamber alters the geometry of each crushing zone in the crushing chamber, resulting in a change in the compression ratio of each crushing zone. As a result, the performance of the cone crusher and the quality of the crushed products are solely affected by variations in the compression ratio of each crushing zone in the crushing chamber, which change with wear.

Combined with Equations (12)–(25), the control point coordinates of the worn concave and the adjusted worn mantle can be obtained, as can the geometry of the adjusted worn crushing chamber. Then, the compression ratio of each crushing zone in the adjusted worn crushing chamber can be determined. By reasonably designing the coordinates of the control points of the mantle and concave, the impact of wear on the change in the compression ratio of each crushing zone in the crushing chamber can be reduced. Thus, the impact of wear on the performance of the cone crusher and the quality of the crushed products are reduced. Therefore, the wear similarity coefficient of the crushing chamber can be established, as shown in Equation (26):

$$\Delta\chi = \frac{\sum_{i=1}^n \sqrt{[(\varepsilon_i - \varepsilon'_i)/\varepsilon_i]^2}}{n} \times 100\% \quad (26)$$

where $\Delta\chi$ is the wear similarity coefficient, ε_i is the compression ratio of the i -th crushing zone, ε'_i is the compression ratio of the adjusted worn i -th crushing zone, and n is the number of the crushing zone in the crushing chamber.

The wear similarity coefficient of the crushing chamber is a dimensionless quantity that describes the difference in the compression ratio between the crushing chamber without wear and the adjusted worn crushing chamber. Therefore, it can be used to define the similarity between the geometry of the crushing chamber, which constantly changes due to wear, and the geometry of the crushing chamber without wear. The constant wear criterion for the crushing chamber of the cone crusher is an optimization method that optimizes the control point coordinates of the mantle and concave to obtain the geometry of the crushing chamber with constant wear characteristics, using the wear similarity coefficient as the optimization objective function. Based on the constant wear criterion, the geometry of the crushing chamber of the cone crusher can be optimized. As the amount of crushed particles increases, the crushing chamber is worn down. The impact of crushing chamber wear on the compression ratio of each crushing zone in the crushing chamber is reduced by adjusting the mantle. The service life of the crushing chamber can be extended based on the premise that the impact of wear on the performance of the cone crusher and the quality of the crushed products can be minimized.

5. Industrial Experiment with ZS200MF Cone Crusher Base on the Constant Wear Criterion

The constant wear criterion can be used to create a new geometry for a crushing chamber or to improve the geometry of an existing crushing chamber in order to achieve a constant wear characteristic. The constant wear characteristic of the crushing chamber helps to reduce the influence of wear on the performance of the cone crusher and the quality of the crushed products, extending the service life of the crushing chamber. In order to verify the feasibility and effectiveness of the constant wear criterion, the performance of the cone crusher and the quality of the crushed products before and after the optimization were compared, and the wear similarity coefficient after optimization was analyzed.

As shown in Figure 12, the ZS200MF cone crusher is a type of ZS-series cone crusher manufactured by the Junyang Machinery Company, Tangshan, China; it is suitable for fine crushing and secondary crushing in small mines. It is equipped with an MF (medium-fine) type crushing chamber, which has a significant market share because of its modular design and cheap operating costs. The ZS200MF cone crusher is a hydraulic cone crusher with a single hydraulic cylinder at the bottom, shown in Figure 8. The concave is fixed on the shell, while the mantle is installed on the main shaft. The particles in the crushing chamber are crushed by the relative squeezing between the mantle and concave caused by the eccentric rotation of the main shaft. As the mantle and concave become worn down, hydraulic oil is injected into the bottom hydraulic cylinder of the cone crusher to adjust the geometry of the crushing chamber. The structural and operating parameters of the ZS200MF cone crusher are shown in Table 3. A ZS200MF cone crusher was erected in a mine in Tangshan, Hebei Province, China. The primary crushed particles consisted of magnetite ore, which has a high iron concentration and is extremely hard. The physical parameters of the crushed magnetite ore are shown in Table 1. The material used for the mantle and concave of the ZS200MF cone crusher is manganese alloy steel, which has high wear resistance. The chemical composition and mechanical properties of the mantle and concave are shown in Tables 4 and 5, respectively.



Figure 12. The ZS200MF cone crusher at the crushing site.

Table 3. The structural and operating parameters of the ZS200MF cone crusher.

Parameter	Unit	Value
Rotational speed (n)	rpm	368
Top diameter of mantle (d_t)	mm	1035
Bottom diameter of mantle (d_b)	mm	404
Base angle of mantle (β)	degree	52
Size of feed port (d_f)	mm	120
Size of output port (f_o)	mm	22
Nip angle (α_n)	degree	31
Length of parallel strip (l_p)	mm	80
Stroke (s)	mm	25
Eccentric distance (e)	mm	12
Eccentric angle (θ)	degree	0.8
Calibration size production (P)	%	75.2

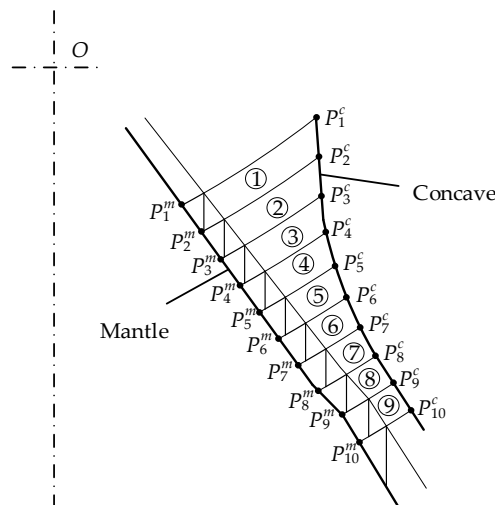
Table 4. The chemical composition of the mantle and concave.

Chemical Element	C	Mn	Si	Cr	Ti	P	S
Content	1.2%	12.7%	0.5%	1.7%	0.05–0.1%	$\leq 0.05\%$	$\leq 0.03\%$

Table 5. The mechanical properties of the mantle and concave.

Parameter	Unit	Value
Yield strength (R_{el})	Mpa	417
Tensile strength (R_m)	Mpa	667
Elongation (A)	%	22
Impact toughness (a_K)	J·cm ⁻²	152
Vickers hardness (HV)	-	527

Based on the developed particle motion characteristic model of the cone crusher, the motion characteristics of particles in the crushing chamber of the ZS200MF cone crusher were simulated and the motion model of particles in the crushing chamber was obtained. Therefore, the crushing chamber was divided into nine crushing zones, with ten control points on the mantle and concave, as shown in Figure 13. The curves between the ten control points on the mantle and concave were replaced by a straight line. The geometry of the crushing chamber of the ZS200MF cone crusher can be simplified to a crushing chamber composed of multiple straight lines. The coordinates of each control point are shown in Table 6.

**Figure 13.** The crushing chamber division of the ZS200MF cone crusher.**Table 6.** The control point coordinates of the mantle and concave.

Control Point	Mantle		Concave	
	x-Coordinate $P_{i,x}^m$	y-Coordinate $P_{i,y}^m$	x-Coordinate $P_{i,x}^c$	y-Coordinate $P_{i,y}^c$
Unit	mm	mm	mm	mm
1	363.7	-614.1	447.5	-556.1
2	380.8	-633.2	451.5	-584.9
3	397.8	-653.1	454.1	-614.3
4	412.8	-672.2	458.1	-642.3
5	426.5	-693.1	464.7	-668.1
6	439.4	-714.4	472.5	-692.9
7	453.7	-734.7	481.4	-716.8
8	468.3	-754.8	491.5	-739.9
9	483.8	-774.3	503.6	-761.6
10	497.4	-794.9	516	-782.9

Based on the constant wear criterion for the crushing chamber of the cone crusher, the mantle and concave of the ZS200MF cone crusher were optimized. According to the structural and operating parameters of the ZS200MF cone crusher, the control point

coordinates of the mantle and concave were optimized within a reasonable range, utilizing the wear similarity coefficient of the adjusted worn crushing chamber as the optimization objective function. The control point coordinates of the optimized mantle and concave are shown in Table 7.

Table 7. The control point coordinates of the optimized mantle and concave.

Control Point	Mantle		Concave	
	x-Coordinate $P_{i,x}^m$	y-Coordinate $P_{i,y}^m$	x-Coordinate $P_{i,x}^c$	y-Coordinate $P_{i,y}^c$
Unit	mm	mm	mm	mm
1	363.7	-614.1	447.5	-556.1
2	379.0	-634.2	449.6	-586.3
3	394.3	-654.3	451.7	-616.1
4	409.5	-674.3	455.1	-644.4
5	424.6	-694.2	462.0	-670.0
6	439.8	-714.1	470.5	-694.3
7	454.9	-734.0	480.6	-717.4
8	470.4	-753.5	492.4	-739.3
9	486.9	-772.4	505.5	-760.3
10	500.1	-793.2	518.7	-781.2

According to the control point coordinates of the optimized mantle and concave based on the constant wear criterion, the mantle and concave with constant wear characteristics were manufactured in cooperation with the Junyang Machinery Company, as shown in Figure 14a,b. The optimized mantle and concave were made of the same materials as the ZS200MF cone crusher. The mantle and concave of the ZS200MF cone crusher were replaced with the optimized mantle and concave with constant wear characteristics. Then, an experimental prototype version of the ZS200MF cone crusher was built. The experimental prototype and the associated equipment were set up at the Junyang Machinery Company, as shown in Figure 14c.

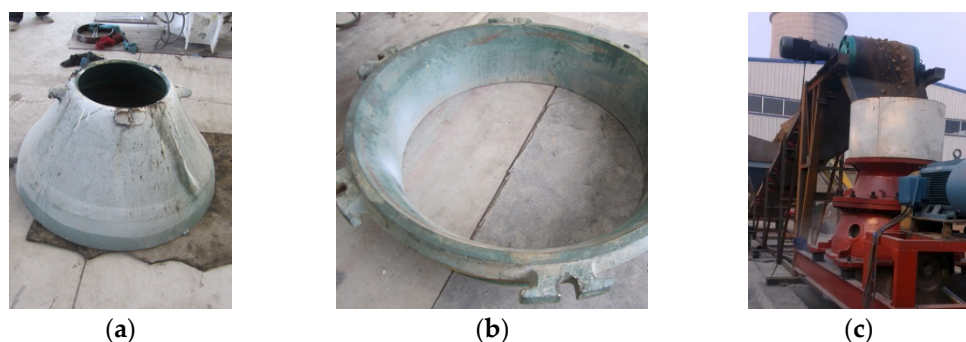


Figure 14. The experimental prototype of the ZS200MF cone crusher with an optimized mantle and concave: (a) the optimized mantle; (b) the optimized concave; (c) the experimental prototype of the ZS200MF cone crusher.

The experimental prototype of the ZS200MF cone crusher was installed and debugged at full power. The industrial experiment lasted for ten days, with a daily operation time of 16 h. The discharge port size of the experimental prototype was adjusted using the suspended lead ball method. The particles crushed in the experimental prototype consisted of magnetite from the mine where the prototype ZS200MF cone crusher was constructed. The experimental process is shown in Figure 15. The capacity of the experimental prototype and the calibration size production of the crushed products were measured once a day, as shown in Table 8. The experimental prototype was turned off and disassembled for inspection every two days. The control point coordinates of the mantle and concave were

measured and the compression ratios of each crushing zone in the crushing chamber were calculated in order to obtain the wear similarity coefficient, which is shown in Table 9.

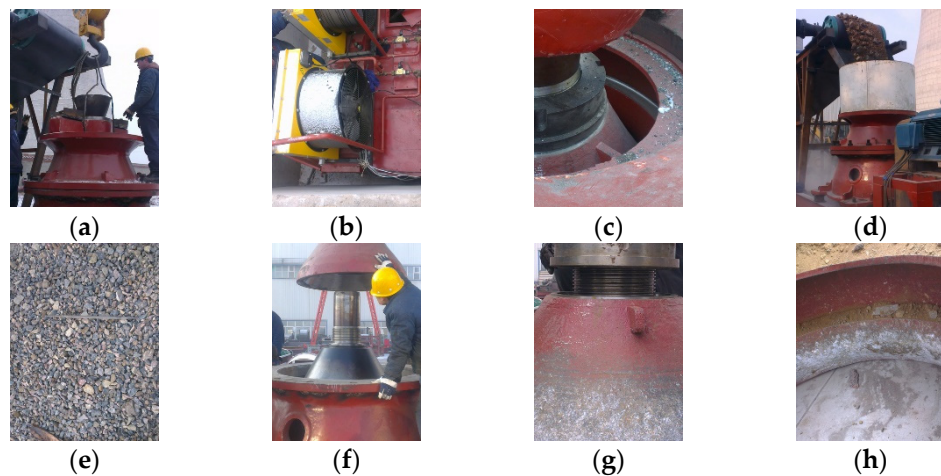


Figure 15. Industrial experiment with the experimental prototype of the ZS200MF cone crusher: (a) the structural parts are installed; (b) the hydraulic system is debugged; (c) the discharge port size is adjusted; (d) the particles are crushed by the experimental prototype; (e) the crushed products obtained per unit time are measured; (f) the experimental prototype is stopped and disassembled for inspection; (g) the worn mantle; (h) the worn concave.

Table 8. The capacity and calibration size production of the experimental prototype.

Parameter	Unit	Value									
Times (T)	d	1	2	3	4	5	6	7	8	9	10
Capacity (C)	t/h	87.8	80.6	88.9	84.9	82.0	80.9	77.2	84.3	84.9	83.0
Calibration size production (P)	%	73.7	79.8	74.9	72.3	73.1	72.6	71.6	70.9	71.1	70.5

Table 9. The wear similarity coefficient of the experimental prototype.

Experiment No.		1	2	3	4	5	6
Times	T	0 d	2 d	4 d	6 d	8 d	10 d
	1	0.14	0.143	0.149	0.156	0.153	0.161
	2	0.169	0.166	0.177	0.183	0.189	0.185
	3	0.209	0.203	0.217	0.213	0.227	0.238
	4	0.251	0.253	0.25	0.26	0.267	0.287
Compression ratios	5	0.295	0.291	0.307	0.315	0.313	0.321
	6	0.339	0.349	0.337	0.348	0.367	0.369
	7	0.379	0.365	0.373	0.379	0.385	0.394
	8	0.406	0.412	0.409	0.413	0.421	0.419
	9	0.421	0.423	0.427	0.426	0.431	0.429
Wear similarity coefficient	$\Delta\chi$	0%	1.95%	2.64%	4.17%	6.46%	8.82%

According to the production records of the ZS200MF cone crusher, the variation in the capacity and calibration size production with the accumulation of the operating time for the ZS200MF cone crusher is shown in Figure 16.

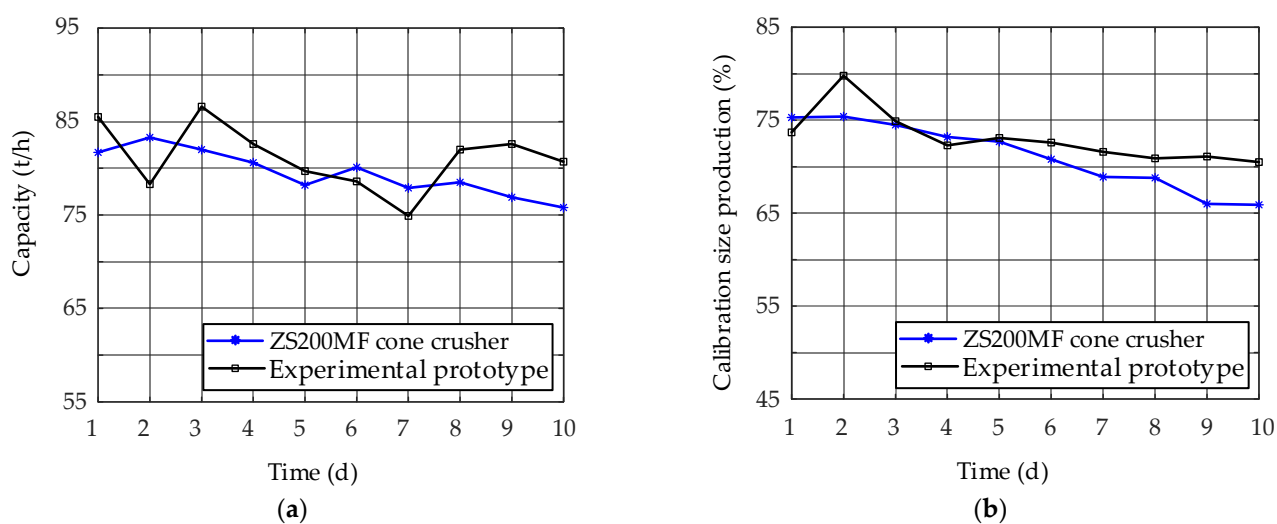


Figure 16. The variation in the capacity and calibration size production of the ZS200MF cone crusher and the experimental prototype: (a) the variation in the capacity and (b) the variation in the calibration size production.

It can be seen from Figure 16a that with accumulating operating time the capacity of the ZS200MF cone crusher gradually decreases, with an average value of 81.8 t/h. The capacity of the experimental prototype fluctuated at an average of 83.45 t/h, and there was no obvious decreasing trend. The difference in average capacity between the ZS200MF cone crusher and the experimental prototype was 1.65 t/h, indicating that using the prototype mantle and concave optimized based on the constant wear criterion had only a small impact on capacity and helped to maintain capacity stability. As shown in Figure 16b, as the operating time increased, the calibration size production of the ZS200MF cone crusher decreased by 9.4%, from 75.3 % to 65.9%, while the calibration size production of the experimental prototype decreased by 3.2%, from 73.7% to 70.5%. The difference in the reduction in calibration size production between the ZS200MF cone crusher and the experimental prototype was 6.2%. This indicates that while the optimized mantle and concave based on the constant wear criterion cannot wholly stop the reduction in the calibration size production with the accumulation of operating time, their use can reduce the degree by which the calibration size production is reduced.

According to the obtained industrial experimental data on the experimental prototype, shown in Table 9, the variation in the compression ratio and wear similarity coefficient with the operating time is shown in Figure 17.

It can be seen from Figure 17a that the compression ratio of the crushing zones had a different degree of increase compared to the initial compression ratio of the crushing zones without wear. Compared to the lower part of the crushing chamber, the compression ratio of the crushing zone in the upper part of the crushing chamber changed significantly. The largest increase in the compression ratio was 0.036, which occurred in crushing zone No. 4 after ten days. The maximum change in the compression ratio was 15.00%, which occurred in crushing zone No. 1 after ten days. From Figure 17b, it can be seen that the wear similarity coefficient of the crushing chamber increased with the accumulation of operating time. When the crushing chamber was operated for ten days, the wear similarity coefficient of the crushing chamber was 8.82%. This indicates that the compression ratio of each crushing zone in the crushing chamber with the optimized mantle and concave based on the constant wear criterion varied less than the standard mantle and concave.

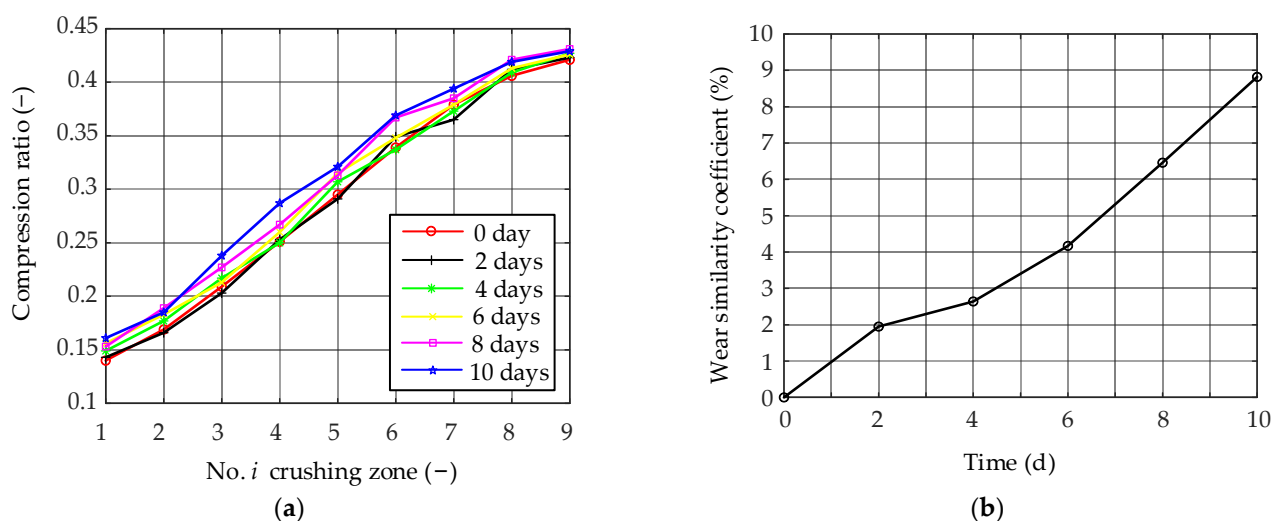


Figure 17. The variation in the compression ratio and wear similarity coefficient of the experimental prototype: (a) the variation in the compression ratio and (b) the variation in the wear similarity coefficient.

According to the path of the particles in the crushing chamber, the crushing chamber of the ZS200MF cone crusher can be divided into several crushing zones in order to obtain the coordinates of the control points of the mantle and concave. Based on the constant wear criterion, the coordinates of the control points were optimized to obtain the mantle and concave with constant wear characteristics. The experimental prototype of the ZS200MF cone crusher was manufactured by replacing the standard mantle and concave with the optimized versions. Productivity, calibration size production, and the wear similarity coefficient were measured during a ten-day industrial experiment using the experimental prototype. Based on our analysis of the industrial experimental data from the experiment prototype, using the optimized mantle and concave based on the constant wear criterion maintains the performance of the cone crusher, delays the eventual decline in crushed product quality, and ensures similarity between the adjusted worn crushing chamber and the initial crushing chamber. Together, this verifies the feasibility and effectiveness of the constant wear criterion for the optimization of crushing chambers.

6. Discussion

The influence of the compression ratio and particle size distribution coefficient on the particle crushing pressure was explored through an experiment involving the particle crushing pressure. A particle crushing pressure model was developed. The particle crushing pressure distribution of the mantle and concave was simulated. According to the particular structure of the cone crusher, the influence of the normal and tangential components of the particle crushing pressure on the wear of the mantle and concave was analyzed. The wear with the increase in particles and accumulated operating time was considered. A wear model of the crushing chamber was established. Analysis of the working process of the cone crusher showed that the bulk properties of the feed and the operating parameters of the cone crusher did not change during the particle crushing process. Therefore, the performance of the cone crusher and the quality of the crushed products are solely related to the changes in the geometry of the crushing chamber caused by wear. A constant wear criterion for the crushing chamber of a cone crusher is proposed here that optimizes the coordinates of the control points of the mantle and concave using the wear similarity coefficient of the adjusted worn crushing chamber as the optimization objective function. The wear similarity coefficient is a dimensionless quantity which characterizes the degree to which the compression ratio of each crushing zone in the crushing chamber, composed of the adjusted worn mantle and the worn concave, deviates from the original value of the compression ratio of each crushing zone in the crushing

chamber without wear. By optimizing the crushing chamber of the cone crusher based on its constant wear characteristics, the geometry of the crushing chamber with constant wear characteristics can be obtained. This reduces the effect of wear on the performance of the cone crusher and on the quality of the crushed products, and extends the service life of the crushing chamber.

Magnetite particles with a size of 25–31.5 mm, which are identical to the particles used for crushing in the ZS200MF cone crusher at the production site, were deliberately selected as the research object of the particle crushing pressure experiment in the theoretical study of the constant wear criterion for the crushing chamber. The adjustment mechanism of the crushing chamber geometry was investigated based on the structural characteristics of the hydraulic cone crusher with a single hydraulic cylinder at the bottom. Thus, the feasibility and effectiveness of the constant wear criterion were sufficiently verified by the industrial experiment with the experimental prototype of the optimized ZS200MF cone crusher. In different industrial sectors, the physical parameters of the crushed products used in cone crushers are different, while various cone crushers have different structural characteristics. As a result, this research cannot be directly applied to the optimization of the crushing chambers of various cone crushers which use various crushed products without modification. However, different cone crushers have similar structural mechanisms, and the crushed products are all brittle. Therefore, the present research can provide inspiration for optimization of the crushing chambers of cone crushers involving different structures and crushed products. The same research method can be used to optimize crushing chambers to obtain a constant wear characteristic.

7. Conclusions

In this paper, the effects of the compression ratio and particle size distribution coefficient on the particle crushing pressure were investigated. The normal and tangential components of the particle crushing pressure on wear were discussed. The increase in wear with the increase in crushed particles and the accumulation of operating time was considered. The adjustment mechanism of the worn mantle was analyzed. Thus, a constant wear criterion for the crushing chamber of the cone crusher was proposed using the wear similarity coefficient as the optimization objective function to obtain a crushing chamber with a constant wear characteristic.

Based on the constant wear criterion, a crushing chamber with the constant wear characteristic was obtained by optimizing the mantle and concave, which was able to reduce the influence of wear on the performance of both the cone crusher and the quality of crushed products, ensuring similarity between the adjusted worn crushing chamber and the initial crushing chamber and thereby extending the service life of the crushing chamber. This research on constant wear criterion offers a theoretical foundation for developing a long-service-life cone crusher or enhancing the wear resistance of the crushing chambers of existing equipment.

Author Contributions: Conceptualization, Z.Z. and T.R.; methodology, Z.Z.; validation, J.C.; formal analysis, Z.Z. and J.C.; investigation, Z.Z. and J.C.; data curation, Z.Z.; writing—original draft, Z.Z.; project administration, T.R. All authors have read and agreed to the published version of the manuscript.

Funding: This work is supported by the National Key Technology R&D Program of China (grant number. 2011BAF15B01).

Data Availability Statement: The data used to support the findings of this study are available from the corresponding author upon request.

Acknowledgments: The authors wish to acknowledge the Junyang Machinery Company, which helped to manufacture the experimental prototype of the ZS200MF cone crusher. The authors especially thank all the people who helped with this subject; because of their aid, this topic was able to be successfully completed.

Conflicts of Interest: The authors declare no conflict of interest.

References

1. Evertsson, C.M. Cone Crusher Performance. Ph.D. Thesis, Chalmers University of Technology, Gothenburg, Sweden, 2000.
2. Lang, B.; Lang, S. *The Cone Crusher*, 1st ed.; China Machine Press: Beijing, China, 1998; pp. 203–207.
3. Archard, J.F. Contact and rubbing of flat surfaces. *J. Appl. Phys.* **1953**, *24*, 981–988. [[CrossRef](#)]
4. Page, N.W.; Yao, M.; Keys, S.; McMillan, W.; Cenna, A.A. A high-pressure shear cell for friction and abrasion measurements. *Wear* **2000**, *241*, 186–192. [[CrossRef](#)]
5. Yao, M.; Page, N.W. Friction measurement on Ni-Hard 4 during high pressure crushing of silica. *Wear* **2001**, *249*, 116–125. [[CrossRef](#)]
6. Yang, J.; Feng, F.; Ma, J.; Shi, J. Wear Law and Parameter Optimization Study on the Split Cone of a Vertical Shaft Impact Crusher. *Math. Prob. Eng.* **2021**, *2021*, 9976571. [[CrossRef](#)]
7. Lindqvist, M.; Evertsson, C.M. Liner wear in jaw crushers. *Miner. Eng.* **2003**, *16*, 1–12. [[CrossRef](#)]
8. Lindqvist, M.; Evertsson, C.M. Prediction of worn geometry in cone crushers. *Miner. Eng.* **2003**, *16*, 1355–1361. [[CrossRef](#)]
9. Lindqvist, M.; Evertsson, C.M.; Chenje, T.W.; Radziszewski, P.H. Influence of particle size on wear rate in compressive crushing. *Miner. Eng.* **2006**, *19*, 1328–1335. [[CrossRef](#)]
10. Lindqvist, M.; Evertsson, C.M. Development of wear model for cone crushers. *Wear* **2006**, *261*, 435–442. [[CrossRef](#)]
11. Dong, G.; Fan, X.M.; Johannesa, N. Modeling crushing pressure and liner wear of cone crusher. *J. Shanghai Jiaotong Univ.* **2011**, *45*, 45–49.
12. Dong, G.; Fan, X.M.; Zhang, X.; Qin, L.H. Crushing force and kinematics analysis of cone crusher based on interparticle breakage. *J. Mech. Eng.* **2010**, *46*, 159–164. [[CrossRef](#)]
13. Reponen, K.P.; Sanna, A.K.; Hellman, J.; Liimatainen, J.; Hannula, S.P. The correlation of material characteristics and wear in a laboratory scale cone crusher. *Wear* **2009**, *267*, 568–575. [[CrossRef](#)]
14. Xu, L.; Luo, K.; Zhao, Y.; Fang, J.; Cen, K. Effect of particle size on liner wear in semi-autogenous mill. *J. Zhejiang Univ.* **2019**, *53*, 2255–2263.
15. Juuso, T.; Kati, V.; Pekka, S.; Veli, K. Correlation of wear and work in dual pivoted jaw crusher tests. *Proc. Inst. Mech. Eng. Part J-J. Eng. Tribol.* **2020**, *234*, 334–349.
16. Liu, R.; Shi, B.; Shen, Y.; Li, G. Prediction model for liner wear considering the motion characteristics of material. *Math. Probl. Eng.* **2018**, *2018*, 9278597. [[CrossRef](#)]
17. Cleary, P.W.; Sinnott, M.D. Simulation of particle flows and breakage in crushers using DEM: Part 1—Compression crushers. *Miner. Eng.* **2015**, *74*, 178–197. [[CrossRef](#)]
18. Cleary, P.W.; Delaney, G.W.; Sinnott, M.D.; Cummins, S.J.; Morrison, R.D. Advanced comminution modelling: Part 1—Crushers. *Appl. Math. Model.* **2020**, *88*, 238–265. [[CrossRef](#)]
19. Sinnott, M.D.; Cleary, P.W. Simulation of particle flows and breakage in crushers using DEM: Part 2—Impact crushers. *Miner. Eng.* **2015**, *74*, 163–177. [[CrossRef](#)]
20. Bengtsson, M.; Hulthén, E.; Evertsson, C.M. Size and shape simulation in a tertiary crushing stage, a multi objective perspective. *Miner. Eng.* **2015**, *77*, 72–77. [[CrossRef](#)]
21. Hulthén, E.; Evertsson, C.M. Algorithm for dynamic cone crusher control. *Miner. Eng.* **2009**, *22*, 296–303. [[CrossRef](#)]
22. Hulthén, E.; Evertsson, C.M. Real-time algorithm for cone crusher control with two variables. *Miner. Eng.* **2011**, *24*, 987–994. [[CrossRef](#)]
23. Li, D.; Wang, Y.; Wang, C.; Li, S. Research on the wear behavior of the fixed cone liner of a cone crusher based on the discrete element method. *ACS Omega* **2020**, *5*, 11186–11195. [[CrossRef](#)] [[PubMed](#)]
24. Duan, G.; Shi, B.; Gu, J. Research of Single-Particle Compression Ratio and Prediction of Crushed Products and Wear on the 6-DOF Robotic Crusher. *Math. Probl. Eng.* **2021**, *2021*, 6634272. [[CrossRef](#)]
25. Magnus, B. Modelling energy and size distribution in cone crushers. *Miner. Eng.* **2019**, *139*, 105869.
26. Zhang, Z.; Ren, T.; Cheng, J. The improved motion model of particles in the cone crusher considering the spatial com-pound motion of the mantle. *Minerals* **2022**, *12*, 16. [[CrossRef](#)]
27. Zhang, Z.; Ren, T.; Cheng, J.; Jin, X. The improved model of inter-particle breakage considering the transformation of particle shape for cone crusher. *Miner. Eng.* **2017**, *112*, 11–18. [[CrossRef](#)]
28. Duarte, R.A.; Yamashita, A.S.; da Silva, M.T.; Cota, L.P.; Euzébio, T.A.M. Calibration and Validation of a Cone Crusher Model with Industrial Data. *Minerals* **2021**, *11*, 1256. [[CrossRef](#)]
29. Yamashita, A.S.; Thivierge, A.; Euzébio, T. A review of modeling and control strategies for cone crushers in the mineral processing and quarrying industries. *Miner. Eng.* **2021**, *170*, 107036. [[CrossRef](#)]
30. Ma, Y.; Fan, X.; He, Q. Wear prediction of multi-material time-varying chamber of cone crusher. *J. Cent. South Univ.* **2016**, *47*, 1121–1127.